

COMPRESSIVE SENSING APPROACH TO HYPERSPECTRAL IMAGE COMPRESSION

K.S. Gunasheela and H.S. Prasantha

Department of Electronics and Communication Engineering, NITTE Meenakshi Institute of Technology, India

Abstract

Hyperspectral image (HSI) processing is one of the key processes in satellite imaging applications. Hyperspectral imaging spectrometers collect huge volumes of data since the image is captured across different wavelength bands in the electromagnetic spectrum. As a result, compression of hyperspectral images is one of the active areas in research community from many years. The research work proposes a new compressive sensing based approach for the compression of hyperspectral images called SHSIR (Sparsification of hyperspectral image and reconstruction). The algorithm computes the coefficients of fractional abundance map in matrix setup, which is used to reconstruct the hyperspectral image. To optimize the problem with non-smooth term existence along with large dimensionality, Bregman iterations method of multipliers is used, which converts the difficult optimization problem into simpler cyclic sequence problem. Experimental result demonstrates the supremacy of the proposed method over other existing techniques.

Keywords:

Hyperspectral Image, Image Compression, Compressive Sensing

1. INTRODUCTION

The HSI is a three-dimensional (3-D) image cube, which is a collection of many two-dimensional (2-D) images. The individual 2-D image is captured at a precise wavelength region in the electromagnetic spectrum. HSI helps us to examine spectral information at every spatial-point in a scene, which helps in identification and classification of materials present in the scene [1]. Hence, hyperspectral imaging is used in many areas such as geology [2], astronomy [3], remote sensing [4] and medical imaging [5]. Even though hyperspectral images have many useful applications, Satellite hyperspectral image processing has some limitations like huge datasets, limited storage availability on board the satellite and limited bandwidth for communication of data to the ground station.

Satellite imaging spectrometers [6] collect huge amount of data, for example if one considers a Megapixel ('106 pixels') camera, which captures some hundred spectral bands in different wavelength region in the electromagnetic spectrum with bit depth equal to 2 bytes. Then, storage and transmission requirement is in terms of gigabytes, which exceeds the available streaming capabilities to transmit the data to ground station. Therefore, the compression of satellite HSI is very much necessary before transmitting the image to ground station. Table.1 contains the list of some of the missions, which collect hyperspectral images across different wavelength regions. There is enormous literature [7] available on algorithms for compression of hyperspectral images. These algorithms are developed to exploit both spatial and spectral correlation in the hyperspectral images. The drawback of these conventional compression method based algorithms is, they

consider all the samples in the image, perform transformation and then do the encoding. These algorithms are computationally expensive. Recent trend is to use compressive sensing approach for the compression, which greatly reduces the number of samples to be considered in an image for reconstruction. Compressive sensing makes use of very less number of samples there by greatly reducing the computational load at the encoder. Moreover, little or no processing is required at the decoder. The memory requirements are also greatly reduced. These characteristics are ideal for satellite image processing applications.

Table.1. Different sensors used in commercial imaging spectrometers

| Sensor | Organization | Country | Number of Bands | Wavelength Range (µm) |
|-----------|--------------------------------|---------------|-----------------|-----------------------|
| AVIRIS | NASA | United States | 224 | 0.4 - 2.5 |
| AISA | Spectral Imaging Ltd. | Finland | 286 | 0.45 - 0.9 |
| CASI | Itres Research | Canada | 288 | 0.43 - 0.87 |
| DAIS 2115 | GER Corp | United States | 211 | 0.4 - 12.0 |
| HYMAP | Integrated Spectronics Pty Ltd | Australia | 128 | 0.4 - 2.45 |
| PROBE-1 | Earth Search Sciences Inc. | United States | 128 | 0.4 - 2.45 |

Apart from many advantages like lower memory requirements, low complexity at encoder side and lower bandwidth requirement for transmission, compressive sensing based algorithms are computationally very expensive at decoder side. This problem can be overlooked as we intend to compress the satellite HSI, where the above mentioned advantages are of greater importance. Compressive sensing is a technique which uses fewer number of samples to reconstruct the data. Compressive samples are taken in a unique fashion by taking inner products with the sensing matrix. The sensing matrix should satisfy some properties for successful reconstruction of the data, like full rank and restricted isometry property [8]. The matrix containing Gaussian i.i.d. entries is used as a sensing matrix which satisfies the above mentioned properties. The data is reconstructed from compressive samples using spectral unmixing and convex optimization techniques in the proposed algorithm.

The main objective of the proposed research is to propose a compressive sensing based methodology to compress and reconstruct the hyperspectral images. The paper demonstrates that reconstruction accuracy and noise robustness of the proposed

algorithm is greatly improved when compared to the state of art algorithms based on compressive sensing based techniques.

The research work proposes a compressive sensing (CS) based algorithm called SHSIR to compress the HSI. The algorithm is developed by assuming linear mixing in hyperspectral images. Reconstruction is performed using Bregman iteration method of multipliers.

2. LITERATURE SURVEY

The necessary condition for any CS based method is sparsity or its compressibility. Many algorithms are proposed under the linear mixing [9] [10] model assumption. Here spectral signatures of pure materials are called end members, which represent the spectral vectors. Coefficients are the abundance fractions of pure materials. The natural images are generally composed of the monotonic objects such as vegetation fields and large buildings. That is why the neighbouring pixels in HSI also represents the similar material. To exploit these features, many algorithms which performs spatial total variation [11] [12] regularization along with unmixing [13] - [19] has been proposed. Chengbo Li et al. [20] uses augmented Lagrangian model to minimize the total variations of abundance fractions. Martin et al. [21] - [23] have developed a strategy called hyperspectral coded aperture to replace the HSI data with a single measurement matrix by computing the inner products between the spectral vectors and known vectors. Chang et al. [24] have redesigned N-FINDR algorithm to reduce the computational complexity and improve the accuracy of extracted endmembers. In [25] the process of unmixing is formulated as a linear regression problem. Guo et al. [26] have used L1 minimization for unmixing the hyperspectral data. In [27] spectral demixing (SD) algorithm is proposed which is similar to Orthogonal matching pursuit, and SD is combined with dictionary learning approach for automatic calculation of endmembers. In [28] spectral unmixing is reformulated as sparse regression problem and a semi supervised optimization approach has been developed to solve the problem. In [29] the application of AMP (Approximate message passing) approach to structural affine rank minimization problems like CS hyperspectral imaging. AMP approach address the complex structures in hyperspectral images which are ignored by affine rank minimization methods. In [30] blind hyperspectral unmixing using Total variation regularization is proposed. The methods in [31] - [33] uses non- blind approach for hyperspectral unmixing. They assume to know the subspace beforehand, which is a noticeable disadvantage related with SpeCA [34], as the recent learns the subspace from the random projections. Compressive-Projection Principal Component Analysis (CPPCA) scheme is introduced in [35] and it is also later on developed in [36]-[38]. The CPPCA algorithm shifts the complexity of PCA from on-board encoder to the base station decoder. Low dimensional Random projections from sensor are sent to the decoder. Decoder finds both the coefficients of PCA transform and approximation to PCA transform basis.

3. HYPERSPECTRAL DATA COMPRESSION AND RECONSTRUCTION

Conventional compression methods first collect the whole dataset, then implements the compression techniques, but the CS

method is different, it directly collects the compressed signal by calculating the inner products between original data and known vectors. This method is called “coded aperture”. There are several approaches to generate the compressed signal from original data. In order to simplify the reconstruction algorithm, the research work uses the following strategy to generate the compressed signal. First, the spatial and spectral domain are decoupled, then Gaussian independent vectors are used to calculate the inner products [39]. The Fig.1 shows the Hyperspectral data compression and decompression. In order to justify the reconstruction of original data from compressed measurement, we minimize the convex objective function that contains 2D total variation regularizer and the quadratic-data eccentric term. This objective function minimization is a difficult optimization problem due to the existence of non-smooth terms and its large-dimensionality. To solve this problem, the Bregman Iteration method of multipliers [40] is adopted to convert a difficult optimization problem into a simpler cyclic sequence problem.

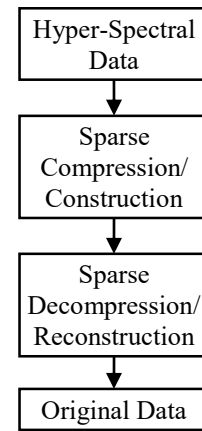


Fig.1. Hyperspectral data compression and reconstruction

Consider a 3D-hyperspectral image in matrix format given by $X \in R^{a_b \times a_p}$, where a_b denotes the number of spectral bands, $a_p = a_r \times a_c$ denotes the number of pixels. a_r and a_c represents the number of rows and columns of hyperspectral image respectively. The X at column side corresponds to the column wise organisation of spectral vectors. The vector measurement by CS is $Y \in R^k$. The measured vector Y can be modelled as:

$$Y = \beta(X) + \mathcal{G} \tag{1}$$

where, β is a linear operator matrix, which calculates k inner values between k known vectors and vectors in X . The element \mathcal{G} corresponds to system noise and modelling errors. The main aim of CS is to reconstruct X from Y with $k \ll a$, $a = a_b \times a_p$. Recovering X is very difficult even in the absence of noise because β is undetermined. If vector x can be represented in some frame ϕ , i.e. $x = \phi\Theta$ where Θ is sparse vector and $x := \text{vec}(X)$. The optimization problem to recover X from Y can be now formulated as:

$$\min_{\Theta} \|\Theta\|_1 \text{ subject to: } \|Y - \beta\phi\Theta\| \leq \zeta \tag{2}$$

where, $\zeta \geq 0$ is the scalar value linked to the noise statistics. Above optimization problem is synthesis based, since we have synthesis prior and we synthesize $x = \phi\Theta$. In [41], L1 regularization using synthesis and analysis priors has been compared. Results indicate the superiority of analysis methods. Hence, we solve Eq.(2) using analysis based method. For that, we introduce an analysis operator

ψ . Transformed vector ψx is sparse. Therefore, Eq.(2) can be written as:

$$\min_x \|\psi x\|_1 \text{ subject to: } \|Y - \beta x\| \leq \zeta \quad (3)$$

In the proposed method, CS is performed in the spectral domain. Different measurement matrices, containing Gaussian i.i.d. entries are used for each pixel. Let p denote the number of measurements to be performed at a particular pixel. Then, $\beta_i \in R^{p \times b}$. Therefore, measurement matrix β can be written in the block diagonal form as:

$$B := B_{dg}(\beta_1, \beta_2, \dots, \beta_{\alpha_p}) \quad (4)$$

where, β_i computes the p projections of vector x_i . Hence, we get $p \times \alpha_p$ measurements and a CR (compression ratio) of α_b/p .

Hyperspectral image consists of hundreds of bands which corresponds to reflectance of the same surface at different narrow regions of the electromagnetic spectrum. Hence, bands in the HSI are highly correlated. Reflectance spectrum at each pixel in an HSI is a mixture of several endmember spectra. Endmembers corresponds to the spectral signatures of a specific material. Fractions of each end members in the spectrum mixture at each pixel location in the HSI is called fractional abundance map.

The Fig.2 illustrates the concept of linear mixing model for HSI. According to linear mixing model, the measured reflectance at a pixel in an HSI is a weighted average of reflectance of materials present in the pixel. Therefore, under the linear mixing model assumption, we can model X as:

$$X = F(T) \quad (5)$$

where, F is the mixing matrix, whose columns corresponds to spectral signatures of end members [42]. $F \in R^{\alpha_b \times g}$ with $g \ll \alpha_b$. T is the fractional abundance map. Entries in T corresponds to fractional abundance coefficients associated with the end members at each pixel location. The estimation of mixing matrix from the ‘original data’ has been done using RMVSA (i.e. Robust minimum value simplex algorithm [43]). It is practical to accept that the estimation of mixing matrix F is done before the data compression. That is why, we are able to reconstruct the T coefficients in the ‘earth station’. During unmixing process, non-negative constraint is imposed on T , i.e. $T \gg 0$.

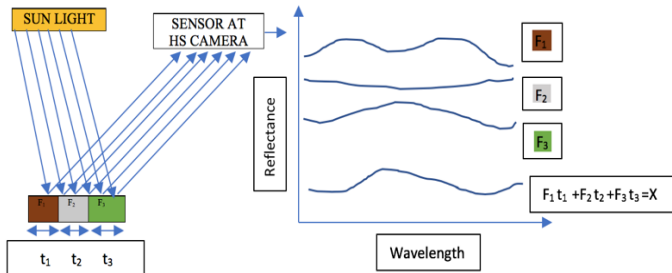


Fig.2. Linear mixing model for HSI

Considering $x = \text{vec}(X)$, $\text{vec}(X) = \text{vec}(FT) = (I_{den} \otimes F)t$ where, $t = \text{vec}(T)$. I_{den} denotes the identity matrix and F is the mixing matrix estimated from the original data. Then, we can write linear operator β on x as:

$$\beta x = \beta(I_{den} \otimes F)t = B_{dg}(\beta_1 F, \dots, \beta_{\alpha_p} F)t \quad (6)$$

Let,

$$W := B_{dg}(\beta_1 F, \dots, \beta_{\alpha_p} F)t \quad (7)$$

Similar to Eq.(3), we can formulate the convex optimization problem to recover the t coefficients as follows:

$$\min_x \|\psi t\|_1 \text{ subject to: } \|Y - Wt\| \leq \zeta \quad (8)$$

Regularizer $\|\psi t\|_1$ is the sum of total variations (V_T) of g images of coefficients T .

$$\|\psi t\|_1 := \sum V_T(T^i) = V_T(t) \quad (9)$$

where, T^i is the i^{th} image coefficient representation with respect to matrix F , therefore, ψ is a discrete gradient operation on T^i .

To obtain piecewise-smooth coefficients of image, we minimize $V_T(t)$. There is a suitable mode to write $V_T(t)$ in terms of the proposed algorithm, as follows:

$$V_T(t) = I(Et) \quad (10)$$

where, I is the given frame and $E := [E_h^r \ E_v^r]^r$ where, E_h and E_v corresponds to $g\alpha_p \times g\alpha_p$ matrices calculating the backward vertical and horizontal differences. Hence, the isotropic total variation regularizer can be defined as:

$$I(Et) = \sum_{j=1}^g \sqrt{(E_{h(i,j)}(t))^2 + (E_{v(i,j)}(t))^2} \quad (11)$$

Isotropic total variation regularizer is chosen because it provides more flexibility regarding the type of discontinuities present in HS-data cubes. According to above mentioned considerations, we are now addressing the following optimization problem.

$$\min_t 0.5\|Y - Wt\|_2^2 + \lambda V_T(t) \text{ subjected to } t \geq 0 \quad (12)$$

The concept of Bregman distance was first introduced in the literature by mathematician L. Bregman [44], where Bregman iterations are used in convex analysis. Later, the method of Bregman iterations are applied to various image processing applications by Stanley Osher et al. [45].

For a constrained minimization problem of the form,

$$\min_u C(u) \text{ such that } Nu = s \quad (13)$$

where $C(u)$ is a convex function. One can find the solution to the above problem by Bregman method as follows, Bregman distance is given by the formula:

$$D_C^{d^L}(u, u^L) = C(G) - C(G^L) - \langle d^L, u - u^L \rangle \quad (14)$$

where, $d^L \in \partial C(u^L)$. By the definition of subdifferentials, $d^L \in \partial C(u^L)$ means that,

$$C(v) - C(u^L) - \langle d^L, v - u^L \rangle \geq 0 \quad \forall v \quad (15)$$

Bregman iterations:

$$u^{L+1} = \arg \min_u D_C^{d^L}(u, u^L) + 0.5\delta \|Nu - s\|^2 \quad (16)$$

$$d^{L+1} = d^L + \delta N^T \|Nu^{L+1} - s\| \quad (17)$$

4. SHSIR ALGORITHM

The main aim of proposed SHSIR algorithm is to compute \hat{T} the matrix setup. Afterwards, we conclude the original ‘hyperspectral’ data by calculating $\hat{X} = F\hat{T}$. The main idea to solve the optimization problem in Eq.(12) is to assign new set of

variables periodically and later we use augmented Bregman-iterations method of multipliers to solve the constrained optimization problem. Equivalent formulation of Eq.(12) is given by,

$$\min_t 0.5\|Y - Wt\|_2^2 + \lambda I(Et) + \iota_{R^+}(t) \quad (18)$$

where, $\iota_{R^+}(t) = \sum_{i=1}^{g\alpha_p} \iota_{R^+}(t_i)$ is an indicator function. t_i corresponds to i^{th} element in t . $\iota_{R^+}(t_i)$ is zero if t_i belongs to non-negative orthant, otherwise it is positive infinity.

Objective function in Eq.(18) can be written the following equivalent form:

$$\min_{t, G_1, G_2, G_3} 0.5\|Y - WG_1\|_2^2 + \iota_{R^+}(G_2) + \lambda I(G_3) \quad (19)$$

subject to: $G_1 = t, G_2 = t, G_3 = E_t$.

In compact form, Eq.(19) can be written as,

$$\min_{t, G} a(G) \text{ subject to: } G = At \quad (20)$$

where,

$$G := [G_1^T, G_2^T, G_3^T]^T \quad (21)$$

$$a(G) = \|Y - G_1\|_2^2 + \iota_{R^+}(G_2) + \lambda I(G_3) \quad (22)$$

where,

$$A = [I_{den}, I_{den}, E]^T \quad (23)$$

To solve the constrained optimization problem Eq.(20), we use adaptive ADMM (Alternating Direction Method of Multipliers). ADMM decomposes the complex optimization problems into cyclic sequence of subproblems. The drawback of ADMM is, we need to manually choose the penalty parameter for the efficient performance of the algorithm. This problem is addressed by AADMM [46], which is completely automated. In our algorithm, we make a small modification to the AADMM by adding Bregman distance to the augmented Lagrangian. Thus, we solve for coefficients t by performing Bregman iterations. Therefore, by problem in Eq.(20) can be reformulated in terms of Bregman-adaptive ADMM iterations as follows:

$$B(t, G, E) \equiv a(G) + D_a^d(G, G^L) + D_a^d(t, t^L) + \frac{\tau}{2} \left\| At - G - E + \frac{\psi_L}{\tau} \right\|^2 \quad (24)$$

where, $D_a^d(G, G^L)$ and $D_a^d(t, t^L)$ are Bregman distances, given by:

$$D_a^d(G, G^L) = a(G) - a(G^L) - \langle d, G - G^L \rangle \quad (25)$$

$$D_a^d(t, t^L) = a(t) - a(t^L) - \langle d, t - t^L \rangle \quad (26)$$

where L represents the iteration. Bregman distance is not a distance by actual means, it actually measures the closeness between G and G^L , t and t^L .

Algorithm 1 (SHSIR)

Initialization: set $L=0$

Select: $\tau \geq 0$

Parameter selection:

$$t^{(0)}, G_1^{(0)}, G_2^{(0)}, G_3^{(0)}, E_1^{(0)}, E_2^{(0)}, E_3^{(0)}, \frac{\psi}{\tau}^{(0)}$$

Parameter updates: Bregman iterations

$$t^{(L+1)} \leftarrow \arg \min_t B(t, G_1^{(L)}, G_2^{(L)}, G_3^{(L)}, E_1^{(L)}, E_2^{(L)}, E_3^{(L)})$$

$$G_1^{(L+1)} \leftarrow \arg \min_{G_1} B(t^{(L+1)}, G_1, G_2^{(L)}, G_3^{(L)})$$

$$G_2^{(L+1)} \leftarrow \arg \min_{G_2} B(t^{(L+1)}, G_1^{(L+1)}, G_2, G_3^{(L)})$$

$$G_3^{(L+1)} \leftarrow \arg \min_{G_3} B(t^{(L+1)}, G_1^{(L+1)}, G_2^{(L+1)}, G_3)$$

Update:

$$E_1^{(L+1)} \leftarrow E_1^{(L)} + t^{(L+1)} - G_1^{(L+1)} + \frac{\psi^{(L)}}{\tau^{(L)}}$$

$$E_2^{(L+1)} \leftarrow E_2^{(L)} + t^{(L+1)} - G_2^{(L+1)} + \frac{\psi^{(L)}}{\tau^{(L)}}$$

$$E_3^{(L+1)} \leftarrow E_3^{(L)} + t^{(L+1)} - G_3^{(L+1)} + \frac{\psi^{(L)}}{\tau^{(L)}}$$

$$d_a^{(L+1)} \leftarrow d_a^{(L+1)} - \tau_{(L)} A^T (At^{(L+1)} - G)$$

Update τ_{L+1} , L until some stopping criterion is satisfied.

The steps involved in SHSIR algorithm is given in Algorithm 1. It is the expansion of Eq.(24). In algorithm 1, the main aim of step 4 (parameter update) is to conclude the variable t value at each iteration. This kind of problem referred to a quadratic problem with block-circulant system matrix, so it is effectively resolved in the Fourier domain.

5. EXPERIMENTAL RESULTS

This section demonstrates the noise robustness and reconstruction ability of the proposed SHSIR algorithm. The proposed algorithm is compared with some existing hyperspectral compressive sensing methods (HCSM) and the simulation has been done using Matlab 2016b. Here the system configurations is 8GB RAM, 1TB ROM, Intel i5 processor, 2GB NVidia Graphics card with the latest operating system of Windows 10.

In this paper, two HSI datasets are selected as the experimental data for the reconstruction of image. They are URBAN [47] and PAVIAU [48]. The URBAN dataset has the dimensions $307 \times 307 \times 210$. It is a 210 bands hyperspectral cube, where each scene comprises of 307×307 pixels. For experimentation, we have cropped the image to 200×200 pixels dimension in each band. The PAVIAU dataset has the dimensions $610 \times 340 \times 103$. It is a 103 bands hyperspectral cube, where each scene comprises of 610×340 pixels. In our experiment, image is cropped to have a dimension of 200×200 pixels in each band. The images are cropped to reduce the computational complexity and time.

In this paper, three state of art HCS based compression techniques are considered for comparison. They are, Orthogonal matching pursuit (OMP [49]), Reweighted Laplace prior based HCS (RLPHCS [50]) and structured sparsity based hyperspectral blind Compressive sensing (SSHBCS [51]). OMP is a greedy sparse learning technique. RLPHCS is a structured-sparsity based sparse learning technique. Both OMP and RLPHCS uses off the shelf dictionaries to sparsify the HSI. SSHBCS is also a structure-sparsity based sparse learning technique but unlike OMP and RLPHCS, SSHBCS performs sparse estimation from

measurements using the learned dictionary. All the above mentioned three state of art models are compared with the proposed model.

To calculate the performance of reconstructed image through different methods, three parameters have been considered. They are Structural similarity index measure (SSIM [52]), Peak signal to noise ratio (PSNR [53]) and Spectral angle mapper (SAM [54]). These parameter measures helps to measure the performance difference between our proposed model and other state of the art techniques which has been considered for comparison. Specifically, PSNR measure indicates the average data similarity between original image reconstructed image. Hence higher PSNR indicates better reconstruction model. SAM measures the average spectral angle between original and reconstructed image at a particular pixel position. Hence smaller SAM values indicates better performance.

The Sampling rate corresponds to the dimension’s proportions of the measurements with respect to the actual HSI. It ranges from 0.1-0.5 in the experiments. The sampling rate is varied from 0.1 to 0.5 to demonstrate the reconstruction capability of the algorithm at various sampling rates. Afterwards, an additive white Gaussian noise is added into the measured HSI with different sampling rate to mimic the noise corruption in hyperspectral compressive sensing (HCS). This gives rise to SNR of 20 dB in the measured HSI.

The algorithm is also verified for reconstruction under different levels of noise with constant sampling rate of 0.4 In the experiments SNR value ranges from 5dB to 40dB to analyse the performance of the algorithm under different levels of noise.

5.1 RECONSTRUCTION AT DIFFERENT SAMPLING RATES AND NOISE LEVEL

The Table.2 shows the PSNR at different sampling rates for the URBAN dataset, similarly Table.4 shows the PSNR at different sampling rates for the PAVIAU dataset. In both cases, sampling rate (SR) varies between 0.1-0.5 at an interval of 0.05 with an additive Gaussian noise of 20dB.

In Table.2, at 0.1 SR the proposed SHSIR model is having 30.75 PSNR value, which is 10.9% more than the SSHBCS, 12.2% more than RLPHCS and 36.59% more than the OMP approach. At 0.5 SR, the SHSIR model is having 43 PSNR value that is 25.23%, 29.35% and 35.16% more compared to the SSHBCS, RLPHCS and OMP model. The average PSNR value of SHSIR algorithm is 37.4 (SR 0.1 to 0.5), which is 17.9%, 21.6% and 26.54% more than the existing model of SSHBCS, RLPHCS and OMP.

Similarly, in Table.4, the average PSNR value of SHSIR algorithm is 50.33 (SR 0.1 to 0.5), which is 36.8%, 39.4% and 44.11% more than the existing model of SSHBCS, RLPHCS and OMP.

Table.2. PSNR at different sampling rates with 20dB noise (URBAN dataset)

| Sampling Rate | 0.1 | 0.15 | 0.2 | 0.25 | 0.3 | 0.35 | 0.4 | 0.45 | 0.5 |
|---------------|------|------|-----------|------|------|------|-----|------|------|
| OMP [20] | 19.5 | 25 | 28.6 7 | 29.8 | 29.6 | 29.3 | 29 | 28.6 | 27.9 |

| | | | | | | | | | |
|-------------|-------|-----------|-----------|-----------|-----------|-----------|-----------|-----------|-----------|
| RLPHCS [21] | 27 | 28.6 4 | 28.6 6 | 29.2 | 29.5 | 30 | 30.2 | 30.4 | 30.4 |
| SSHBCS [22] | 27.4 | 29.5 6 | 29.9 8 | 30.8 | 30.8 4 | 31.5 | 31.8 | 32.3 | 32.1 5 |
| SHSIR | 30.75 | 32.1 6 | 34 | 35.8 5 | 37.8 | 39.2 9 | 41.2 5 | 42.5 8 | 43.0 3 |

Table.3. SAM at different sampling rates with 20dB noise (URBAN dataset)

| Sampling Rate | 0.1 | 0.15 | 0.2 | 0.25 | 0.3 | 0.35 | 0.4 | 0.45 | 0.5 |
|---------------|-------|-------|-------|------|------|-------|------|-------|------|
| OMP [20] | 18.75 | 13.9 | 10.8 | 9.7 | 10.5 | 10.62 | 11 | 11.38 | 12.2 |
| RLPHCS [21] | 11.2 | 10.32 | 10.51 | 9.96 | 9.8 | 9.44 | 9.21 | 8.8 | 8.95 |
| SSHBCS [22] | 9.7 | 8.4 | 8.35 | 7.3 | 7.49 | 7 | 7.1 | 6.4 | 6.8 |
| SHSIR | 11 | 8.56 | 6.7 | 5.15 | 4.23 | 3.44 | 2.6 | 2.21 | 2.07 |

Table.4. PSNR at different sampling rates 20dB noise (PAVIAU dataset)

| Sampling Rate | 0.1 | 0.15 | 0.2 | 0.25 | 0.3 | 0.35 | 0.4 | 0.45 | 0.5 |
|---------------|-------|-----------|-------|-----------|-----------|-----------|-----------|-----------|-----------|
| OMP [20] | 22.14 | 25.3 | 30.75 | 30 | 29.3 7 | 29.5 2 | 29.3 8 | 28.6 2 | 28.1 1 |
| RLPHCS [21] | 27.6 | 28.8 1 | 30.76 | 30.7 4 | 31 | 31.1 9 | 31.4 5 | 31.4 4 | 31.4 6 |
| SSHBCS [22] | 27.8 | 29.5 6 | 32.23 | 32.2 | 32.4 5 | 32.8 5 | 33.0 8 | 33 | 33.1 4 |
| SHSIR | 43.95 | 46.5 4 | 48.11 | 49.7 9 | 50.6 | 52.0 9 | 52.9 3 | 53.9 3 | 55.0 7 |

Table.5. SAM at different sampling rates with 20dB noise (PAVIAU dataset)

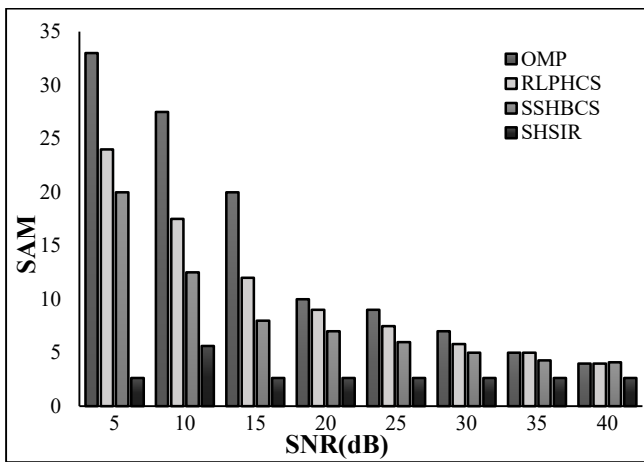
| Sampling Rate | 0.1 | 0.15 | 0.2 | 0.2 5 | 0.3 | 0.35 | 0.4 | 0.45 | 0.5 |
|---------------|-----------|-----------|----------|----------|----------|-----------|----------|-----------|----------|
| OMP [20] | 17.6 2 | 12.5 1 | 8.1 1 | 9.7 | 10. 5 | 10.6 2 | 11 | 11.3 8 | 12. 2 |
| RLPHCS [21] | 9.7 | 8.9 | 7.8 | 7.8 2 | 7.4 5 | 7.3 | 7 | 7.05 | 6.9 |
| SSHBCS [22] | 8.8 | 7.3 | 5.7 | 5.8 2 | 5.7 1 | 5.47 | 5.3 | 5.4 | 5.2 2 |
| SHSIR | 1.82 | 1.34 | 1.1 4 | 0.9 4 | 0.8 5 | 0.72 | 0.6 5 | 0.58 | 0.5 1 |

The Table.3 shows the SAM values at different sampling rates for the URBAN dataset, similarly Table.5 shows the SAM values at different sampling rates for the PAVIAU dataset. In Table.3, at 0.1 SR the SAM value of SHSIR is 11.05 that is 12.2% more than the SSHBCS, 1.3% and 41% less than the RLPHCS and OMP respectively. We can clearly observe that SSHBCS performs better at 0.1 and 0.15 SR, other than that, our proposed model performs considerably well from 0.2 to 0.5 SR value. The average SAM value of SHSIR algorithm for URBAN data set is 5.12 (SR

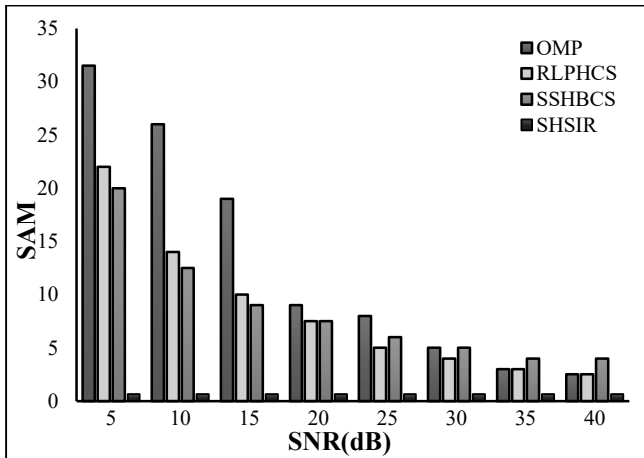
0.1 to 0.5), which is 32.79%, 47.7% and 57.6% less than the existing model of SSHBCS, RLPHCS and OMP.

Similarly, in Table.5, at 0.1 SR, the proposed SHSIR model is having 1.8 SAM value, which is 79% less than the SSHBCS, 81% less than RLPHCS and 89.6% less than the OMP approach. The average SAM value of SHSIR algorithm for PAVIAU data set is 0.95 (SR 0.1 to 0.5), which is 84.3%, 87.7% and 91.7% less than the existing model of SSHBCS, RLPHCS and OMP.

The Fig.3(a) shows the SAM versus noise level bars for the URBAN dataset, similarly Fig.3(b) shows the SAM versus noise level bars for the PAVIAU dataset. In both cases sampling rate is kept constant i.e. 0.4. The Gaussian noise added is varied from 5 dB to 40dB to analyze the performance of algorithm at different noise levels. The average SAM value of SHSIR algorithm for URBAN data set is 2.62 (SNR 5dB to 40dB), which is almost three times, four times, seven times less than the existing model of SSHBCS, RLPHCS and OMP.



(a)



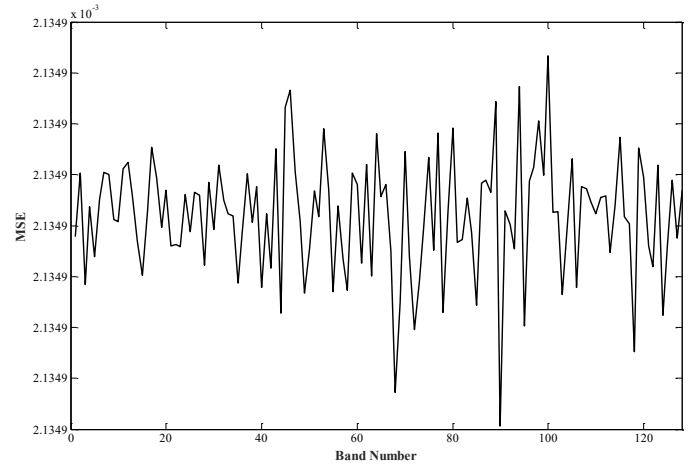
(b)

Fig.3. SAM vs. noise level bars (a) URBAN dataset, (b) PAVIAU dataset

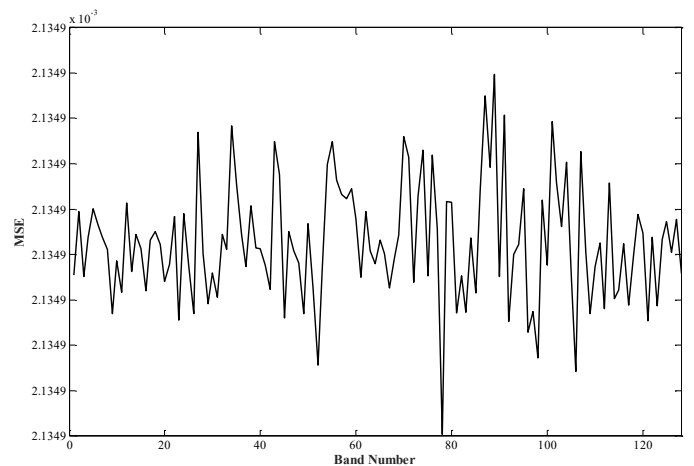
Similarly, in Fig.3(b), the average SAM value of SHSIR algorithm for PAVIAU data set is 0.6547 (SNR 5dB to 40dB), which is thirteen times less than SSHBCS and RLPHCS model, and almost 20 times less than average SAM value in OMP model.

The Fig.4(a) shows the MSE (Mean Square Error) with respect to the different bands in the URBAN dataset. When the

measurement SNR is 20 dB and the sampling rate is 0.2, the error in reconstruction using SHSIR algorithm is more close to zero, which can be seen in Fig.4(a) and the average value of MSE from 0 to 128 band is 0.0021, the maximum variation is seen in 90th and 100th band. Similarly, Fig.4(b) shows the MSE with respect to the different bands in the URBAN dataset at 0.4 sampling rate. Here also the error rate is closer to zero that can be seen in Fig.4(b), the maximum variation is seen in 78th and 88th band and, the average value of MSE is 0.0021.



(a)



(b)

Fig.4. MSE at different band numbers (a) URBAN dataset (0.2 Sampling rate), (b) URBAN dataset (0.4 Sampling rate)

6. CONCLUSION

The research work proposes a new framework for the compression of hyperspectral data acquired in compressive sensing fashion. The proposed SHSIR algorithm takes benefit of the two main hyperspectral data properties, such as the high spatial correlation between abundance fractions and less number of end members, required to represent the data. The main constraint of SHSIR algorithm is computation time since we are dealing with huge hyperspectral datasets. We overlook the computation time for the reconstruction, as it happens in the ground station where resources are available in abundance. The improvement in the performance is obtained because we have incorporated RMVSA algorithm for endmember extraction,

which increases the accuracy in endmember extraction. Another main reason for better performance of our algorithm is, we have used Bregman solver to solve the optimization problem, which advances the reconstruction accuracy of the original HSI data set. The proposed algorithm is compared with state of art CS based compression algorithms. Experimental results demonstrate the supremacy of the proposed technique over other state of art techniques.

REFERENCES

- [1] D.C. Heinz and C.I. Chang, "Fully Constrained Least-Squares Linear-Spectral Mixture Analysis Approach for Material Quantification in the Hyperspectral Imagery", *IEEE Transactions on Geoscience and Remote Sensing*, Vol. 39, No. 3, pp. 529-545, 2001.
- [2] F.A. Kruse, J.W. Boardman and J.F. Huntington, "Comparison of Airborne Hyperspectral Data and EO-1 Hyperion for Mineral Mapping", *IEEE Transactions on Geoscience and Remote Sensing*, Vol. 41, No. 6, pp. 1388-1400, 2003.
- [3] E.K. Hege, D. O'Connell, W. Johnson, S. Bastay and E.L. Dereniak, "Hyperspectral Imaging for Astronomy and Space Surveillance", *Proceedings of 48th Annual Meeting Optical Science and Technology*, pp. 380-391, 2004.
- [4] M.E. Schaepman, S.L. Ustin, A.J. Plaza, T.H. Painter, J. Verrelst and S. Liang, "Earth System Science related Imaging Spectroscopy-An Assessment", *Remote Sensing of Environment*, Vol. 113, pp. 123-137, 2009.
- [5] S.V. Panasyuk et al., "Medical Hyperspectral Imaging to Facilitate Residual Tumor Identification during Surgery", *Cancer Biology and Therapy*, Vol. 6, No. 3, pp. 439-446, 2007.
- [6] N. Gat, "Imaging Spectroscopy using Tunable Filters: A Review", *Proceedings of SPIE*, Vol. 4056, pp. 50-64, 2000.
- [7] K.S. Gunasheela and H S Prasantha, "Satellite Image Compression-Detailed Survey of the Algorithms", *Proceedings of International Conference on Cognition and Recognition*, Vol. 14, pp. 187-198, 2017.
- [8] E. Candes and T. Tao, "Decoding by Linear Programming", *IEEE Transactions on Information Theory*, Vol. 51, No. 12, pp. 4203-4215, 2005.
- [9] S. Alliney and S.A. Ruzinsky, "An Algorithm for the Minimization of Mixed l1 and l2 Norms with Application to Bayesian Estimation", *IEEE Transactions on Signal Processing*, Vol. 42, pp. 618-627, 1994.
- [10] R. Tibshirani, "Regression Shrinkage and Selection via the Lasso", *Journal of the Royal Statistical Society: Series B*, Vol. 58, pp. 267-288, 1996.
- [11] L.I. Rudin, S. Osher and E. Fatemi, "Nonlinear Total Variation based Noise Removal Algorithms", *Physica D: Nonlinear Phenomena*, Vol. 60, No. 1-4, pp. 259-268, 1992.
- [12] A. Chambolle, "An Algorithm for Total Variation Minimization and Applications", *Journal of Mathematical Imaging and Vision*, Vol. 20, pp. 89-97, 2004.
- [13] J.M. Bioucas-Dias and M.A.T. Figueiredo, "A New Twist: Two-Step Iterative Shrinkage/Thresholding Algorithms for Image Restoration", *IEEE Transactions on Image Processing*, Vol. 16, No. 12, pp. 2992-3004, 2007.
- [14] J.L. Starck, M. Elad and D.L. Donoho, "Image Decomposition via the Combination of Sparse Representations and a Variational Approach", *IEEE Transactions on Image Processing*, Vol. 14, No. 7, pp. 1570-1582, 2005.
- [15] A. Beck and M. Teboulle, "Fast Gradient-based Algorithms for Constrained Total Variation image Denoising and Deblurring Problems", *IEEE Transactions on Image Processing*, Vol. 18, No. 11, pp. 2419-2434, 2009.
- [16] M.V. Afonso, J.M. Bioucas Dias and M.A.T. Figueiredo, "Fast Image Recovery using Variable Splitting and Constrained Optimization", *IEEE Transactions on Image Processing*, Vol. 19, No. 9, pp. 2345-2356, 2010.
- [17] M. V. Afonso, J. M. Bioucas-Dias, and M. A. T. Figueiredo, "An Augmented Lagrangian Approach to the Constrained Optimization Formulation of Imaging Inverse Problems", *IEEE Transactions on Image Processing*, Vol. 20, No. 8, pp. 681-695, 2011.
- [18] T. Goldstein and S. Osher, "The Split Bregman Method for L1-Regularized Problems", *SIAM Journal on Imaging Sciences*, Vol. 2, pp. 323-343, 2009.
- [19] J.M. Bioucas-Dias, M.A.T. Figueiredo and J.P. Oliveira, "Total Variation-based Image Deconvolution: A Majorization-Minimization Approach", *Proceedings of International Conference on Acoustics Speech and Signal Processing*, pp. 1-4, 2006.
- [20] Chengbo Li, T. Sun, K.F. Kelly and Y. Zhang, "A Compressive Sensing and Unmixing Scheme for Hyperspectral Data Processing", *IEEE Transactions on Image Processing*, Vol. 21, No. 3, pp. 1200-1210, 2012.
- [21] G. Martin, J.M. Bioucas-Dias and A. Plaza, "HYCA: A New Technique for Hyperspectral Compressive Sensing", *IEEE Transactions on Geoscience and Remote Sensing*, Vol. 53, No. 5, pp. 2819-2831, 2015.
- [22] G. Martin, J.M. Bioucas-Dias and A. Plaza, "Hyperspectral Coded Aperture (HYCA): A New Technique for Hyperspectral Compressive Sensing", *Proceedings of 21st European Signal Processing Conference*, pp. 1381-1384, 2012.
- [23] G. Martin, J.M.B. Dias and A.J. Plaza, "A New Technique for Hyperspectral Compressive Sensing using Spectral Unmixing", *Proceedings of International Conference on Society for Optics and Photonics*, pp. 551-556, 2012.
- [24] Chein I Chang, Chao-Cheng Wu and C.T. Tsai, "Random N-finder (N-FINDR) Endmember Extraction Algorithms for Hyperspectral Imagery", *IEEE Transactions on Image Processing*, Vol. 20, No. 3, pp. 641-656, 2011.
- [25] K.E. Themelis, A.A. Rontogiannis and K.D. Koutroumbas, "A Novel Hierarchical Bayesian Approach for Sparse Semisupervised Hyperspectral Unmixing", *IEEE Transactions on Signal Processing*, Vol. 60, No. 2, pp. 585-599, 2012.
- [26] Z. Guo, T. Wittman and S. Osher, "L1 Unmixing and its Application to Hyperspectral Image Enhancement", *Proceedings of International Conference on Algorithms and Technologies for Multispectral, Hyperspectral, and Ultraspectral Imagery*, pp. 1181-1192, 2009.
- [27] J.B. Greer, "Sparse Demixing of Hyperspectral Images", *IEEE Transactions on Image Processing*, Vol. 21, No. 1, pp. 219-228, 2012.

- [28] M.D. Iordache, J.M. Bioucas-Dias and A. Plaza, "Sparse Unmixing of Hyperspectral Data", *IEEE Transactions on Geoscience and Remote Sensing*, Vol. 49, No. 2, pp. 2014-2039, 2011.
- [29] Y. Li, C. Yin, W. Chen and Z. Han, "Approximate Message Passing for Structured Affine Rank Minimization Problem", *IEEE Access*, Vol. 5, pp. 10093-10107, 2017.
- [30] J. Sigurdsson, M.O. Ulfarsson and J.R. Sveinsson, "Blind Hyperspectral Unmixing using Total Variation and L_q Sparse Regularization", *IEEE Transactions on Geoscience and Remote Sensing*, Vol. 54, No. 11, pp. 6371-6384, 2016.
- [31] C. Li, T. Sun, K. Kelly and Y. Zhang, "A Compressive Sensing and Unmixing Scheme for Hyperspectral Data Processing", *IEEE Transactions on Image Processing*, Vol. 21, No. 3, pp. 1200-1210, 2011.
- [32] M. Golbabaee, S. Arberet and P. Vandergheynst, "Compressive Source Separation: Theory and Methods for Hyperspectral Imaging", *IEEE Transactions on Image Processing*, Vol. 22, No. 12, pp. 5096-5110, 2013.
- [33] G. Martin, J. Bioucas-Dias and A. Plaza, "HYCA: A New Technique for Hyperspectral Compressive Sensing", *IEEE Transactions on Geoscience and Remote Sensing*, Vol. 53, No. 2, pp. 2819-2831, 2014.
- [34] Jose M. Bioucas-Dias et al., "Hyperspectral Unmixing Overview: Geometrical, Statistical, and Sparse Regression-Based Approaches", *IEEE Journal of Selected Topics in Applied Earth Observations and Remote Sensing*, Vol. 5, No. 2, pp. 354-379, 2012.
- [35] J. Fowler, "Compressive-Projection Principal Component Analysis", *IEEE Transactions on Image Processing*, Vol. 18, No. 10, pp. 2230-2242, 2009.
- [36] J.E. Fowler and Q. Du, "Reconstructions from Compressive Random Projections of Hyperspectral Imagery", *Optical Remote Sensing*, pp. 31-48, 2011.
- [37] C. Chen, W. Li, E. Tramel and J. Fowler, "Reconstruction of Hyperspectral Imagery from Random Projections using Multihypothesis Prediction", *IEEE Transactions on Geoscience and Remote Sensing*, Vol. 52, No. 1, pp. 365-374, 2014.
- [38] W. Li, S. Prasad and J. Fowler, "Integration of Spectral-Spatial Information for Hyperspectral Image Reconstruction from Compressive Random Projections", *IEEE Geoscience and Remote Sensing Letters*, Vol. 10, No. 6, pp. 1379-1383, 2013.
- [39] J.E. Candes, T. Romberg and T. Tao, "Robust Uncertainty Principles: Exact Signal Reconstruction from Highly Incomplete Frequency Information", *IEEE Transactions on Information Theory*, Vol. 52, No. 2, pp. 489-509, 2006.
- [40] C. Wu and X.C. Tai, "Augmented Lagrangian Method, Dual Methods and Split Bregman Iteration for ROF, Vectorial TV, and High Order Models", *SIAM Journal on Imaging Sciences*, Vol. 3, No. 3, pp. 300-339, 2010.
- [41] I.W. Selesnick and M.A.T. Figueiredo, "Signal Restoration with Overcomplete Wavelet Transforms: Comparison of Analysis and Synthesis Priors", *Proceedings of SPIE Optical Engineering*, pp. 1-15, 2009.
- [42] Gabriel Martin and Jose. M. Bioucas-Dias, "Hyperspectral Blind Reconstruction from Random Spectral Projections", *IEEE Journal of Selected Topics in Applied Earth Observations and Remote Sensing*, Vol. 9, No. 6, pp. 2390-2399, 2016.
- [43] A. Agathos, J. Li, J. M. Bioucas-Dias and A. Plaza, "Robust Minimum Volume Simplex Analysis for Hyperspectral Unmixing", *Proceedings of 22nd European Signal Processing Conference*, pp. 1582-1586, 2014.
- [44] L.M. Bregman, "A Relaxation Method of Finding a Common Point of Convex Sets and its Application to the Solution of Problems in Convex Programming", *USSR Computational Mathematics and Mathematical Physics*, Vol. 7, No. 3, pp. 200-217, 1967.
- [45] W. Yin, S. Osher, D. Goldfarb and J. Darbon, "Bregman Iterative Algorithms for l_1 Minimization with Applications to Compressed Sensing", *SIAM Journal on Imaging Sciences*, Vol. 1, No. 1, pp. 143-168, 2007.
- [46] Zheng Xu, Mario A.T. Figueiredo and Tom Goldstein, "Adaptive ADMM with Spectral Penalty Parameter Selection", *Proceedings of International Conference on Artificial Intelligence and Statistics*, Vol. 54, pp. 718-727, 2017.
- [47] Hyperspectral Remote Sensing Scenes, Available at: http://www.ehu.es/ccwintco/index.php/Hyperspectral_Remote_Sensing_Scenes
- [48] J.A. Tropp and A.C. Gilbert, "Signal Recovery from Random Measurements via Orthogonal Matching Pursuit", *IEEE Transactions on Information Theory*, Vol. 53, No. 12, pp. 4655-4666, 2007.
- [49] L. Zhang, W. Wei, Y. Zhang, C. Tian and F. Li, "Exploring Structural Sparsity by a Reweighted Laplace prior for Hyperspectral Compressive Sensing", *IEEE Transactions on Image Processing*, Vol. 25, No. 10, pp. 4974-4988, 2016.
- [50] L. Zhang, W. Wei, Y. Zhang, C. Shen, A. Van Den Hengel and Q. Shi, "Dictionary Learning for Promoting Structured Sparsity in Hyperspectral Compressive Sensing", *IEEE Transactions on Geoscience and Remote Sensing*, Vol. 54, No. 12, pp. 7223-7235, 2016.
- [51] Z. Wang, A.C. Bovik, H.R. Sheikh and E.P. Simoncelli, "Image Quality Assessment: From Error Visibility to Structural Similarity", *IEEE Transactions on Image Processing*, Vol. 13, No. 5, pp. 600-612, 2004.
- [52] Y. Peng, D. Meng, Z. Xu, C. Gao, Y. Yang and B. Zhang, "Decomposable Nonlocal Tensor Dictionary Learning for Multispectral Image Denoising", *Proceedings of IEEE Conference on Computer Vision and Pattern Recognition*, pp. 2949-2956, 2014.
- [53] R.H. Yuhas, J.W. Boardman and A.F.H. Goetz, "Determination of Semi-Arid Landscape Endmembers and Seasonal Trends using Convex Geometry Spectral Unmixing Techniques", *Proceedings of 4th Annual JPL Airborne Geoscience Workshop*, Vol. 1, pp. 205-208, 1993.